Journal Pre-proof

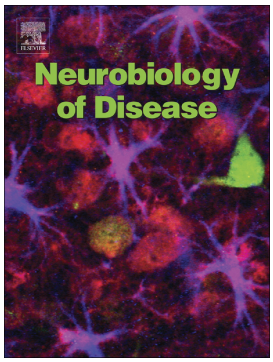

Eight cylindrical contact lead recordings in the subthalamic region localize beta oscillations source to the dorsal STN

Idit Tamir, Doris Wang, Witney Chen, Jill L. Ostrem, Philip A. Starr, Coralie de Hemptinne

PII: S0969-9961(20)30365-X

DOI: https://doi.org/10.1016/j.nbd.2020.105090

Reference: YNBDI 105090

To appear in: *Neurobiology of Disease*

Received date: 10 April 2020

Revised date: 20 September 2020

Accepted date: 21 September 2020

Please cite this article as: I. Tamir, D. Wang, W. Chen, et al., Eight cylindrical contact lead recordings in the subthalamic region localize beta oscillations source to the dorsal STN, *Neurobiology of Disease* (2020), https://doi.org/10.1016/j.nbd.2020.105090

This is a PDF file of an article that has undergone enhancements after acceptance, such as the addition of a cover page and metadata, and formatting for readability, but it is not yet the definitive version of record. This version will undergo additional copyediting, typesetting and review before it is published in its final form, but we are providing this version to give early visibility of the article. Please note that, during the production process, errors may be discovered which could affect the content, and all legal disclaimers that apply to the journal pertain.

© 2020 Published by Elsevier.

Journal Pre-proof

Eight cylindrical contact lead recordings in the Subthalamic region localize beta oscillations source to the dorsal STN

Idit Tamir[a,b,*] Iditta1@clalit.org.il**, Doris Wang**[a]**, Witney Chen**[a]**, Jill L Ostrem**[c]**, Philip A Starr**[a]**, Coralie de Hemptinne**[a]

[a]Philip Starr Laboratory**,** Department of Neurosurgery, University of California, San Francisco, California, USA

[b]Department of Neurosurgery, Rabin Medical Center, Petach Tikva, Israel (present address)

[c]Department of Neurology, University of California, San Francisco, California, USA

[*]**Corresponding author at:** Department of Neurosurgery, Rabin Medical Center, 39 Zabotinski St., Petach Tikva, Israel

***** Color should be used for all figures**

***** Conflict of interest:**

Jill Ostrem and Philip Starr received grant support from Boston Scientific as part of the Intrepid phase III clinical trial

Other authors have no conflict of interest to declare

Journal Pre-proof

Journal Pre-proof

Abstract

Background: In Parkinson's disease (PD) patients, the subthalamic nucleus (STN) has prominent oscillatory activity in the beta band, which may be related to the motor symptoms severity. Local field potential (LFP) studies using standard four-contact deep brain stimulation (DBS) leads indicate that the source of beta activity in the STN region is the dorsolateral segment of the nucleus. However, these leads have few contacts outside of the STN, making the source localization of beta activity around the STN region uncertain.

Objective: This study aimed to investigate the electrophysiological characteristics of the STN and the surrounding area in PD to better locate the source of these oscillations and their clinical relevance.

Methods: Eight PD patients were bilaterally implanted in the STN with the eight ring-contact DBS lead (Boston Scientific Corporation). LFPs were recorded intra-operatively from each DBS contact in the off medication state at rest. Each contact location was normalized relative to the STN borders based on microelectrode recordings. For each recording, power spectral density was computed, averaged over multiple frequency bands and phase reversal analysis was used to localize the source of oscillatory activity. Beta burst, high-frequency activity (HFA), and phase-amplitude coupling (PAC) were also computed. Neurophysiological signatures were correlated with hemibody symptoms severity and clinical outcomes.

Results: Beta band power and phase reversal localized the beta oscillator to the dorsal STN and correlated with pre-operative off medication hemibody bradykinesia and rigidity score.

Journal Pre-proof

The contact along the electrode with the largest beta oscillatory power co-localized with the independently chosen optimized contact used for long-term chronic DBS. Lastly, beta bursting, HFA, and Beta-HFA PAC co-localized with the beta oscillator at the dorsal STN, and Beta-HFA PAC correlated with DBS effect.

Conclusions: Our findings support the hypothesis that the primary source of beta oscillations is located in dorsal STN, and argue against the alternative hypothesis that beta activity in the STN region arises from volume conduction from other sources. We demonstrate intrinsic STN beta-HFA PAC as an independent marker of DBS effect.

Keywords: DBS; STN; Parkinson's disease; Beta oscillation; PAC; HFA; Beta burst; cross-frequency coupling; subthalamic nucleus; deep brain stimulation.

Journal Pre-proof

Introduction

Abnormal synchronization of neuronal activity throughout the basal ganglia thalamocortical loop has been associated with dysfunction of the motor circuits in PD. In particular, beta oscillations (13-35 Hz) are prominent in the parkinsonian STN local field potential (LFP) activity in both humans (Shreve et al. 2017) and non-human primates (Deffains et al. 2016; Wichmann, Bergman, and DeLong 2018). Beta activity is suppressed both by dopaminergic medication and DBS (Sharott et al. 2005; Galati et al. 2009; Hohlefeld et al. 2013; Lourens et al. 2013; Pollok et al. 2013; Toledo et al. 2014; West et al. 2016) and the degree of suppression correlates with PD patients' severity of rigidity and bradykinesia (Hohlefeld et al. 2013; Toledo et al. 2014; West et al. 2016). Besides beta spectral power, studying the dynamic characteristics of these oscillations has revealed the role of beta bursts in PD. A higher incidence of longer bursts was found in the off medication state, and correlated with motor symptoms severity (Tinkhauser, Pogosyan, Little, et al. 2017; Tinkhauser, Pogosyan, Tan, et al. 2017). Coupling between the phase of beta oscillations and the amplitude of high-frequency activity (HFA, also called High Frequency Oscillations, HFOs, in some publications) is also thought to play a role in the pathophysiology of PD (Ozkurt et al. 2011; Lopez-Azcarate et al. 2010; Shreve et al. 2017). Beta oscillations may represent a biomarker of the parkinsonian state in PD, and a possible candidate control signal for adaptive stimulation algorithms, adjusting stimulation based on a physiological biomarker of disease state (Tinkhauser, Pogosyan, Little, et al. 2017; Deffains and Bergman 2019; Pina-Fuentes et al. 2019).

The source of these beta oscillations is thought to be localized to the dorsal portion of the STN (Alavi et al. 2013; Lourens et al. 2013; Feng et al. 2016), while lower frequency bands dominate

the ventral portion of the nucleus (Eitan et al. 2013; Kolb et al. 2017; Rappel et al. 2018). However, prior studies have utilized either monopolar recordings using a macro contact of the microelectrode or bipolar recordings using the standard four contact DBS leads (Pogosyan et al. 2010; Marmor et al. 2017; Kolb et al. 2017), with no simultaneous sampling from inside and outside the borders of the STN.

Here, we recorded and analyzed for the first time bipolar LFPs along an eight cylindrical contact DBS lead, with a total array length spanning 15.5 mm to provide spatially accurate comparisons of the biophysical characteristics of the ventral and dorsal parts of the STN to those outside of the STN. Using this novel method, we found the maximal beta power, maximal PAC, larger and longer beta bursts, and phase reversal of the beta waveform to be highly localized in the dorsal portion of the STN, indicating that the source of beta oscillations at the STN vicinity is localized to the dorsal STN. We also found the disease symptoms to correlate with beta activity and the DBS-related effect on motor symptoms to correlate with Beta-HFA PAC. The contacts used for chronic stimulation co-localized with the Beta activity and Beta-HFA PAC. These novel findings suggest multiple markers that may drive adaptive stimulation paradigms to help tighter patient symptom control and improve DBS outcomes.

Journal Pre-proof

Methods

Study Patients, Clinical Assessment Scales, and Inclusion Criteria

Eight patients were included in this intraoperative study and gave written informed consent. All of them were also enrolled in the INTREPID Study (Implantable Neurostimulator for the Treatment of Parkinson‘s disease), a double blind-sham stimulation controlled study that aims to test the safety and efficacy of bilateral STN stimulation through a new fractionated contact current DBS system with an 8 contact linear lead (Vercise™ system; Boston Scientific Corporation; Valencia, CA).

Patients were recruited from the movement disorder surgery clinic at the University of California, San Francisco (UCSF). All patients had a diagnosis of bilateral idiopathic Parkinson's disease with at least 5 years of motor symptoms, including at least 2 of the following: resting tremor, rigidity, or bradykinesia.

Motor impairment was assessed preoperatively (during the month before the date of operation) and postoperatively (at weeks 4, 8, 12, 20, 26, 48, 52 and 78 after treatment randomization/ post-operative baseline visit) by movement disorders neurologists using the Unified Parkinson's Disease Rating Scale part III (UPDRS-III) in the off and on medication state. All patients’ pre-operative off medication UPDRS part III score was 30 or higher, and they had disabling PD features (either off time or on time with troublesome dyskinesia) for at least six hours a day. Patients’ demographic and motor scores are shown in table 1. The hemibody scores were determined using the UPDRS III by adding contralateral limb sub-scores for rigidity and bradykinesia in the off medication state preoperatively. The cognitive and mental functions were assessed in detail by a neuropsychologist before surgery. Independently optimized DBS

parameters at one year were noted for each hemisphere. The Vercise pulse generator allows the fractionalization of cathodal current across multiple contacts. In cases of bipolar or double monopolar programming with asymmetric fractionalization, the location of the cathode activated at >50% was chosen for correlations. If two contacts were used equally (50% each) in a double monopolar mode, then the average location of the two was used. This study was in agreement with the Declaration of Helsinki and was approved by the institutional ethics committee.

DBS surgery and lead implantation

Eight cylindrical contacts DBS leads (Vercise™ system; Boston Scientific Corporation; Valencia, CA) were implanted in awake patients targeting the STN as previously described (Starr 2002). For pre-operative planning, volumetric MRI (either 1.5 or 3 Tesla) was conducted prior to surgery, including T1+gadolinium, T2, and FGATIR sequences. The dorsolateral STN was then directly targeted on the MRI. Microelectrode recording (MER) was performed to identify dorsal and ventral borders of the STN, including identification of movement-related single-cell discharges to indicate the motor territory of the STN. After the STN was mapped based on MER and at least a 5mm segment of the STN was identified, an 8 cylindrical contact Boston Scientific DBS lead (lead configuration: 1.3 mm in diameter, 8 cylindrical contacts with 1.5 mm contact length and 0.5 mm contact spacing) was placed with at least 2 contacts within the STN, as defined by MER map. Contacts were labeled 1 to 8, from ventral to dorsal. We targeted the dorsal border of the third contact to the dorsal border of the STN (as defined by MER).

Intraoperative test stimulation was performed to determine the therapeutic window (clinically significant symptom improvement without stimulation-induced adverse effects. If the therapeutic

window was too narrow, the lead was repositioned. The final lead placement was confirmed by intraoperative (O-arm; Medtronic Inc., Minneapolis, Minnesota) and postoperative high-resolution CT fused to the preoperative MRI (Figure 1a) (Shahlaie, Larson, and Starr 2011).

LFP recordings

All patients were off-medication (antiparkinsonian medications held 12 hours) at the time of surgery, resting with eyes open, immediately after lead insertion and before test stimulation. The Alpha Omega Microguide Pro (Alpha Omega, Inc., Nazareth, Israel) was used for MER, and LFPs were recorded in a monopolar configuration, sampled at a frequency of 22000 Hz. Data were re-referenced to a bipolar configuration using adjacent contacts offline. In 4 patients LFPs were recorded bilaterally while in the other 4 patients LPFs were recorded from the most affected side, resulting in recordings from 12 hemispheres.

Identification of STN borders and electrode contact location

Given the variability in the patient's STN size and DBS contact location within this structure, the STN length was normalized and contacts were localized relative to the STN borders. This normalization allows statistical analyses across patients and was done as follows: The dorsal and ventral STN borders along the lead trajectory were determined based on the MER recordings intra-operatively. The resulting length of the STN along the recording track was normalized so that, for each patient, the ventral border was defined as '0', and the dorsal border as '1'. Five zones were then defined based on the normalized STN and named as follows: zone 1 - relative

distance of 0-0.5, representing ventral STN; zone 2 - relative distance of 0.5-1, representing dorsal STN; zone 3 – relative distance of 1-1.5, just dorsal to the STN; zone 4 – relative distance 1.5-2, dorsal to zone 3; zone 5 – relative distance >2, dorsal to zone 4.

To determine the location of each bipolar local field potential, the center of each DBS contact pair was then localized relative to this normalized trajectory (figure 1B). This normalization allowed us to study the differences in electrophysiological signals across patients. Although these 'zones' approximately correspond to the structures identified with the 3D Schaltenbrand Wahren Atlas superimposed on the pre-operative MRI (e.g., zone 1 - ventral STN, zone 2 - dorsal STN, zone 3 - Zona Incerta, zone 4 - White Matter, and zone 5 - Reticular Thalamus), we did not attempt to localize structures outside of the STN using individualized MRI features. For comparison of various electrophysiological properties across the five normalized locations (zones), averaging of values originating in the same zone was warranted (i.e., if two bipolar contact pairs were localized to the dSTN, averaging between the values of these two was conducted to compare it to values of the same parameter in other locations like vSTN).

Data recording and filtering

All analyses were performed offline using Matlab version 2017b software (Mathworks Inc., Natick, MA). To obtain better spatial localization and reduced noise, LFPs recorded from each contact in a monopolar fashion were re-referenced to its adjacent contact (C1-C2, C2-C3, etc...). All major recording artifacts (including line noise at 60Hz and harmonics) were filtered using a notch filter (Butterworth, 3rd order) of 6 Hz width around the peak artifact frequency.

All LFP data was downsampled to 1000 Hz. The first 30s of data without obvious electrical noise or movement were selected for analysis. Sweeps were reviewed individually to exclude those with visible artifacts. Out of 84 bipolar re-referenced channels, ten were noisy and therefore excluded from the analysis.

Power spectral analysis

In the resting condition, *Power spectral density* (PSD) was calculated for each bipolar contact pair using a fast Fourier transform and the Welch periodogram method with a 1 s Hanning window and a 0.5 overlap to reduce edge effects, to create a frequency resolution of 1 Hz. Frequencies under 3 Hz were excluded from the analysis. The calculated PSD values were transformed into a logarithmic scale for all statistical comparisons. To correct for differences in baseline broadband power across patients, PSDs were normalized. The absolute power at each frequency band was divided by the averaged 'baseline' power at 140-160 Hz of the same contact pair. We used this method for all frequency bands, except for 200-400 Hz activity used for evaluation of HFA. The band of 140-160 Hz was chosen for normalization as there was no peak activity or artifacts at this band in any of the patients, and it seems to fairly represent baseline 'background power' of each contact.

For statistical analyses, the PSDs were then averaged over multiple frequency bands (theta (5-7 Hz), alpha (8-12 Hz), beta (13-30 Hz), low beta (13-20 Hz), high beta (20-30 Hz), gamma (30-50 Hz), broadband activity (50-200 Hz), and high-frequency activity (HFA, 200-400 Hz)). In

addition to averaged power, contacts with the maximal power in each frequency band were also identified.

For HFA, the frequency with the highest power (spectral peak frequency; local elevation of power in the spectra) was visually inspected and manually chosen, and the averaged power around the peak (50 Hz in width) was taken and then divided by the baseline power, similarly to the other frequency bands. In cases where a clear peak was not obvious, the average power of the total HFA bandwidth was used. This method was used due to the variability in peak frequency in the HFA band across patients and states, as well as the narrow nature of the peak (50 Hz) relative to the bandwidth chosen (200-400 Hz), as previously reported (van Wijk et al. 2016).

Beta burst analysis

To quantify bursts of beta oscillatory activity, we used methods previously described (Tinkhauser, Pogosyan, Tan, et al. 2017; Tinkhauser, Pogosyan, Little, et al. 2017). Beta band peaks were individually visually identified on log spectral power density plots. Each LFP signal (of each contact and each patient) was band-pass filtered (±4 Hz) around individual beta peak frequency, and the amplitude envelope of the Beta activity was obtained. A threshold was then set at the 75th percentile of the beta amplitude. The onset of a burst was defined as when the filtered signal crossed the threshold amplitude and the end of the burst defined as when the amplitude fell below threshold (Tinkhauser, Pogosyan, Tan, et al. 2017). This burst identification method was felt to be applicable because variations in beta power across contacts were not extreme (Schmidt et al. 2020). Bursts lasting less than 100 ms were discarded from the analysis.

Amplitude and duration of each burst were calculated, as well as the mean amplitude and duration of bursts for each contact. These were then compared across lead contacts to identify (in each lead) the contact with maximal burst amplitude or duration, and correlate it with Beta power.

Beta phase reversal analysis

To localize the source of beta oscillations, a phase reversal analysis was performed using circ_stat Matlab toolbox (Berens, 2009). The signal was band-pass filtered in a 5 Hz band bin around the Beta peak of each patient lead. The instantaneous phase angle of the beta bandpass filtered signal was calculated using the Hilbert transform for each bipolar contact pair. The phase difference between two adjacent contact pairs (bipolar contact-the adjacent bipolar contact; for example, contact 1-2 minus contact 2-3, etc...) was calculated using circ_dist. 'The mean vector length computed based on all beta phase difference vectors, representing the variation of the data around the mean, was calculated by circ_r and plotted. Uniformity of phase data was tested by the Rayleigh test (circ_rtest) using the circ_stat toolbox for Matlab (Berens, 2009).

Phase reversal was evaluated using the circ_vtest to compare the phase difference from each neighboring contact pairs to 180 degrees (defined as the absolute reversal). In this test, the significance of reversal is determined based on the non-uniformity of the distribution of phases around a specific angle which is not significantly different than 180 degrees. (Kombos et al. 1999). The location of the contact common for both pairs was then defined as the location of the

reversal. Thus if phase reversal was found between bipolar contact 2-3 and bipolar contact 3-4, then contact 3 was defined as the source of beta oscillations.

Phase-amplitude coupling

Phase-amplitude coupling indices were quantified using a method previously described (Canolty et al. 2006; Tort et al. 2010). First, LFPs were band-pass filtered at low (from 2 to 50 Hz in 2Hz steps with a 2Hz bandwidth, without overlap) and high frequencies (from 50 to 400 Hz in 4Hz steps with a 4Hz bandwidth, without overlap) using a FIR1 filter (eeglab). Second, the instantaneous phase and the instantaneous amplitude were extracted from the low and the high frequency filtered signal, respectively, after applying the Hilbert transform. The instantaneous phase was divided into bins of 20° and distribution of the instantaneous amplitude envelope was computed for each bin. The phase-amplitude coupling (Modulation Index; MI) was then determined by computing the entropy values of this distribution and normalizing by the maximum entropy value. For each contact pair, the coupling between each frequency for phase and amplitude was computed and represented on a modulation index plot.

For each cotact pair of each patient, the overall magnitude (*PAC mean*) of cross-frequency coupling was determined by averaging the coupling between phases extracted from the 13-30 Hz band and amplitudes extracted from the 200-400 Hz band.

To avoid artifactual coupling across frequency bands as was described previously in the literature (Tort et al. 2010; Gerber et al. 2016; Cole et al. 2017; Hyafil 2017; Zhong et al. 2017; Scheffer-Teixeira and Tort 2017), we used a permutation test to determine the significance of derived MI values. We computed the distribution of 500 surrogate data for each pair of

frequencies by adding a temporal random offset to the amplitude signal. Assuming that the surrogate data follow a normal distribution, we used a p-value of 0.01 (99th percentile) to get the significance threshold value of the derived MI values.

Statistical analysis

All statistical analyses were performed in Matlab. Regression plots were created either in Matlab or SigmaPlot (version 14.0, Systat Software Inc., San Jose, CA, USA). Comparisons of power and PAC values between contact pairs and relative locations of contacts were performed using non-parametric ANOVA on ranks (Kruskal-Wallis test; does not assume a normal distribution of data and applies to repeated measures). Post-hoc Dunn-Sidak test was used to correct for multiple comparisons. For paired comparisons, we used the Wilcoxon non-parametric sign rank test, given the low number of patients. Correlations between the various clinical and electrophysiological parameters were performed using Spearman correlation. Unless specified otherwise, a significance level of 0.05 was used throughout the analysis. Correction for the false discovery rate was conducted using Benjamini & Hochberg test. The circ_stat Matlab toolbox was used for phase-related statistical analysis.

Journal Pre-proof

Results

We enrolled 8 (5M/3F) patients into this study and recorded the oscillatory activity of LFPs recorded from 12 STNs (4 bilateral and 4 unilateral). Patients' demographics and PD-related clinical data are summarized in Table 1.

Figure 1A shows an example of a lead location in the STN area. A T2 weighted image in the axial plane at the level of the red nucleus fused with the post-operative CT scan shows the implanted leads intersecting the dorsolateral STN. Figure 1B shows a 3D image (based on the pre-op MRI fused with the post-operative CT scan) of the entire lead trajectory traversing the STN area. Fig 1C shows an example of all bipolar contacts' power spectral densities (PSDs; without normalization) of one lead, between 1-200 Hz. Differences in baseline power at all frequency bands were seen between the contacts located at and around the STN (Fig. 1C, C1-3) and the contacts located dorsal to it (C4-7). Grouping all patients' non-normalized data and comparing baseline power between the five zones of relative contact locations yielded a significant difference in baseline power (best seen at frequency range 140-160 Hz were no peaks in power are evident) ($p<0.001$, non–parametric ANOVA). Contacts located within the STN (vSTN and dSTN) had higher baseline power than contacts dorsal to the STN (zones 4-5; $p<0.05$, post hoc Dunn-Sidak tests). Zone 3 location had an intermediate power between the STN and the more dorsal locations which did not differ from the other zones. These differences in baseline power may represent the cellular density, similar to the increase in background activity when traversing the STN with a microelectrode (as illustrated in Fig. 2A). Due to these differences in baseline power across contacts, the signal was normalized (see Methods and Fig.

1D) in each patient to eliminate this shift in broadband power and emphasize the differences in peak power of low frequencies.

Beta oscillations are maximal at the dorsal Subthalamic Nucleus

Figure 1D shows an example of normalized log PSDs for STN field potentials recorded from each adjacent DBS contact pair from one trajectory of a patient. A peak of power in the beta band is evident, especially in contact pair 3-4, located in this patient at the dorsal STN. For this trajectory, the maximal beta power was found in the dorsal STN, as shown in Figure 1E illustrating in a 4D plot the spatial localization (in AC-PC coordinates) of STN averaged beta power of each contact pair. In all patients, the beta power was maximal at the dorsal STN area or slightly dorsal to the STN border (Table 2). These estimate 'bipolar' locations were within 0.14-0.2 from the real lead contact locations. The lengths of the lead trajectories within the STN and the number of lead contacts implanted within the nucleus are also mentioned in Table 2. The number of lead contacts within the STN was a result of the exact location of the contact centers (used for this analysis) in relation to the STN borders, and the overall depth of the lead in relation to the STN borders. Therefore, in some leads, fewer contacts are located within a longer STN trajectory.

Given the variability in STN length and contact location across patients (see Table 2), the contact location was normalized to the STN borders. Figure 2B shows the averaged PSD recorded from each 'zone' across patients (red color, PSD±SEM Fig. 2B). Group analysis reveals that beta power was different between zones ($p=0.00004$, KW test; Fig. 2C). Beta power was higher at the dorsal STN (dSTN beta power median and range: 1.22(0.7-2.3)) compared with recordings dorsal to the STN (zone 4 (0.65(0.2-1.4)) and zone 5 (0.48(0.4-1)). As a group, beta power in the

dSTN was not different from the ventral STN (1.19(0.5-2)) or zone 3 (0.88(0.4-1.9), Fig. 2C). Nevertheless, most patients (9/12) had their maximal Beta power at the dorsal STN contacts (Fig. 2D).

Beta phase reversal localizes oscillator to the Subthalamic nucleus

In clinical neurophysiology, the source of electrical activity is often detected by the 'phase reversal', i.e., the reversal of the polarity of the electrical signal between the two sides of the activity generator. We, therefore, studied the 'phase reversal' of beta-band oscillations across contact pairs. Figure 3A shows an example of one patient's 500 ms epoch signal, recorded from bipolar contact pairs, band-pass filtered to the beta peak frequency. The phase reversal in this example occurs between bipolar contacts 1 and 2 (indicated by the arrow).

The mean and distribution of phase differences between contact pairs in the different locations were plotted, as well as the phase vector, representing the 'strength' of the preferred phase reversal angle. In the exemplary patient shown in Figure 3B, the phase reversal was found between contact pairs 1-2 and 2-3, suggesting contact 2 as the location of the oscillator. In this case, contact 2 was found to be in the STN (relative location 0.34).

In most patients, the beta phase reversal was found to be within the dorsal STN (7 of 12 leads; Fig. 3C). In the other 5 leads, the reversal was found very close to the dorsal STN borders, either at the vSTN or zone 3. Interestingly, the localization of beta phase reversal to the dorsal STN corresponded to the localization of the maximal beta power (0.88(1.3); r^2=0.76, p=0.0001; Spearman correlation). Taken together, these data suggest the dorsal STN as the origin of beta

oscillations, and rules out the alternative of a distal generator recorded locally due to volume conductance.

Other potential PD biomarkers are localized to the dorsal STN

Given recent recognition that beta activity tends to occur in bursts (Tinkhauser, Pogosyan, Little, et al. 2017; Tinkhauser, Pogosyan, Tan, et al. 2017), we identified the contact with the maximal burst amplitude and duration and for each contact, averaged all burst events. The lead contacts with the largest amplitude beta bursts were localized to the dSTN in 10 of 12 leads (Fig. 4A, left), while the contacts with the longest bursts were more widespread (vSTN to zone 4) with only 6 leads at the dSTN (Fig. 4A, right). Beta bursts were recently found to time lock HFA (Meidahl et al. 2019). This was suggested as the mechanism of coupling of the amplitude of HFA to the phase of the beta rhythm, which may be relevant to the pathophysiology of PD (Lopez-Azcarate et al. 2010; van Wijk et al. 2017). Here we found a positive correlation between HFA power and burst amplitude (r^2=0.46, p=0.01, Fig. 4B), but not duration (data not shown). Most STNs (8 of 12) showed at least one contact pair with significant beta-HFA coupling. An example of STN PAC is illustrated in figure 4C. The maximal PAC value located at the dorsal STN (6 of 8, Fig. 4DE). Similarly, a spectral peak at the HFA band (200-400 Hz;) was found in most patients (8/12 STNs; (67%)) with a median peak frequency of 265+/- 100 Hz (all STN trajectories). A representative example from one patient (same patient as Figure 1) is shown in Fig. 4E. While the peak HFA frequency in all patients was preserved across contact locations, the power intensity varied significantly (p=0.0036, KW test) with the largest HFA amplitude located in the dorsal STN (data not shown). Most patients had their maximal HFA power at the dorsal STN border (Fig. 4F).

The maximal beta-HFA PAC of all patients (often located in dorsal STN) was positively correlated with the maximal HFA power (r^2=0.27, p=0.04; data not shown) but not with the maximal beta power (r^2=0.06, p=0.23; data not shown). Nevertheless, the location of maximal PAC was strongly correlated with the location of maximal beta power (r^2=0.69, p=0.004; Fig. 4G) as well as the location of the beta phase reversal (r^2=0.46, p=0.02; data not shown). In addition, the maximal PAC (of each lead) was strongly correlated with the contralateral delta UPDRS on-off stimulation (r^2=0.45, p=0.01; Fig.4H) Taken together, these data suggest that HFA is intrinsic to the STN, and couples with beta bursting at the dorsal STN. This coupling is an independent predictor of the effect of DBS.

DBS targets the Beta oscillator

Eleven of twelve active contacts used for chronic stimulation across patients were in the STN, while the remaining one was in zone 3. Among the active contacts located to the STN, 9 were found at the dorsal STN and only two contacts at the ventral STN (Fig. 5A).

Beta power at the contact used for stimulation of each patient's STN trajectory was positively correlated with off-medication pre-operative contralateral bradykinesia and rigidity (r^2=0.36, p=0.02; Fig. 5B). No correlation was found between Beta power at the stimulation contact and tremor severity (r^2=0.002, p=0.88, data not shown). Additionally, no correlation was found between Beta power at other contact locations and symptom severity (data not shown). Taken together, these data implicate that the optimal target for the DBS contact can be predicted from the location of the contact with maximal beta power. These data are in agreement with similar findings in the literature (Neumann et al. 2016; Chen et al. 2010).

Journal Pre-proof

Discussion

Summary

We used recordings from a DBS lead with eight cylindrical contacts spanning 15.5 mm to evaluate the anatomic localization of oscillatory phenomena in the subthalamic region. These data suggest beta oscillations to be intrinsic to the dorsal STN, to co-localize with the target for chronic stimulation and to correlate with contralateral bradykinesia and rigidity severity in these patients. We also show HFA and cross-frequency coupling between the beta phase and HFA amplitude within the dorsal STN. The beta-HFA PAC in the STN co-localizes with the beta oscillator (determined by beta power and phase) and correlates with the DBS effect.

Beta source localization

Despite many studies recording and analyzing beta oscillations in the STN, few have addressed localization of this marker in simultaneous high channel count recordings (Alavi et al. 2013; Lourens et al. 2013; Toledo et al. 2014; Hohlefeld et al. 2015; Verhagen et al. 2015; Kolb et al. 2017; Marmor et al. 2017). While most studies used 3 bipolar contacts spreading along the STN itself, we used an octopolar lead in which the contacts spread way beyond the STN borders. This is the first study to assess the topography of beta characteristics using DBS leads with double the channel count.

We utilized a normalization technique for localizing the lead contacts in the STN, compensating for inter-patient variation of lead trajectory and STN anatomy (Tamir et al. 2017). Using phase reversal methods and others, we localized the beta oscillations to the dorsal STN, and found

correlations between beta activity and the patients' motor state, as previously reported. Beta power was significantly larger in the STN than in the more dorsal contacts. However, no significant difference was found between dorsal and ventral areas of the STN. The similarity within the STN fit previous findings (Alavi et al. 2013) and probably result from high STN synchronization in the Parkinsonian state and volume conduction in the STN itself. The finding of lower Beta power dorsal to the STN supports the STN as the generator of beta oscillations that synchronizes both input and output BG nuclei and argues against other beta sources that may transmit the beta signal by volume conduction (Plaha et al. 2006). The oscillations of the STN may be responsible for synchronizing BG activity to generate automatic and reflex motor patterns necessary for movement and function. In Parkinson, there may be a deficit in the top-down regulation of the basal ganglia activity by the motor cortex (Tommasi et al. 2015; Deffains and Bergman 2019), disrupting goal-driven fine movements that require strict cortical control. Nevertheless, our findings do not prove the STN to be the sole independent generator of beta oscillation, as other potential sources interconnected with the STN are not excluded in this study.

Beta oscillations as a biomarker for akinetic-rigid PD motor severity

Our findings highlight the strong association between STN beta oscillations and the motor impairment of these patients. Beta oscillations are a well-characterized feature of the dorsal STN in PD. (Zaidel et al. 2010; Little and Brown 2012; Rosa et al. 2011) . While beta oscillations are probably normal phenomena in brain physiology (Buzsaki and Draguhn 2004), excessively synchronized beta activity in the BG circuitry is believed to be the hallmark of the hypo-dopaminergic state (Zaidel et al. 2010; Wang et al. 2018; van Wijk et al. 2017; Horn et al.

2017)). Our results are in agreement with prior literature indicating a correlation between the amplitude of resting-state STN beta oscillations and the severity of bradykinesia and rigidity (Chen et al. 2010; Neumann et al. 2016; West et al. 2016).

Other potential Biomarkers

Basal Ganglia HFA and its coupling to the beta phase have been previously described in PD patients. Van Wijk et al (van Wijk et al. 2017) studied the source for high-frequency activity and beta-HFA PAC at the STN and reported a slightly more dorsal location for these markers compared to beta power. In this study, we found a strong correlation between the location of Beta power and PAC, although the intensity of Beta power and PAC were not correlated, hinting for two independent markers co-occurring in the same location. Beta-HFA PAC has been shown to correlate with disease severity (Ozkurt et al. 2011; Yang et al. 2014; Sanders and Jaeger 2016; Shreve et al. 2017; van Wijk et al. 2016) In our study, PAC correlated best with DBS effect on UPDRS. However, the origin and functional role of these findings in PD are still under debate (Foffani et al. 2003; Lopez-Azcarate et al. 2010). Recently, STN HFA has been suggested to reflect hyper-synchronization of single-cell spiking activity, and beta-HFA PAC to reflect locking of spiking activity to network beta oscillations (Meidahl et al. 2019). The same study also showed increased beta-HFA coupling during prolonged and robust beta bursts. Our findings are in agreement with this literature and strengthen the association between HFA and beta bursts.

The finding of potential biomarkers like PAC, HFA, and beta bursting at the DBS target has important implications and can potentially be used for better targeting of the DBS lead and as a

detection signal for adaptive stim strategies. Future studies aim to test these hypotheses are warranted.

Study Limitations

The method we used to localize the electrode contacts is based on the MER and is not anatomical. It enables only 2D localization in the plane of the DBS trajectory and assumes accurate placement of the lead at the intended depth such that its location is "registered" with the MER map. In addition, using 'bipolar' referencing also for contact localization reduces accuracy of presumed contact location.

We use UPDRS part III measured a few weeks pre-operatively and not intra-operative motor evaluation for correlations with intraoperatively recorded electrophysiological markers. However, the severity of symptoms might be altered during surgery by anesthesia and electrode insertion lesion effects. These might affect the reported correlations.

Phase reversal analysis showed STN as the source of Beta oscillations but was unable to define the dorsal part of the nucleus as the oscillator. While the borders between the dorsal 'motor' and the postero-ventral 'associative' area of the nucleus are not well defined to date, previous studies showed an equal length of ventral and dorsal STN in a typical STN lead trajectory (Tamir et al. 2017). However, the relative span of 'motor' vs. 'non-motor' parts of the STN also depends on the DBS lead trajectory. Limbic areas of the STN are located anteromedial of the intended DBS trajectory and were not well represented in this study. Therefore, 'vSTN' in this study might include 'motor' STN as well.

Journal Pre-proof

We suggest dSTN as the sole generator of Beta oscillations in the STN vicinity. Nevertheless, this study did not include recordings of other regions of the BG-thalamocortical networks. Therefore, we cannot exclude the existence of additional beta oscillators, or a distant main oscillator in the BG-thalamo-cortical network, although previous studies do not support this hypothesis.

Journal Pre-proof

Figure Legends

Table 1. Patient Demographics Study's patients' age, Years from diagnosis of Parkinson's disease at the time of surgery, gender, total pre-operative off medications UPDRS part III, a pre-operative subscore for rigidity and bradykinesia and intra-operative subthalamic nucleus side recorded are described. Abbreviations: STN=Subthalamic nucleus, Meds=medications, YRS=years, UPDRS=Unified Parkinson's Disease Rating Scale, R=right, L=left, PT=patient, op=operative, BR=bradykinesia, and rigidity.

Figure 1. Beta oscillatory activity at the Subthalamic Nucleus of DBS implanted Parkinson's Disease patients. A. Pre-operative axial T2 MRI image at the level of the red nucleus (red), co-localized with the postoperative CT. A typical location of the DBS electrode (green) implanted bilaterally is demonstrated. **B.** A 3D scheme of the lead trajectory in relation to the various anatomical structures as reconstructed from the pre-op MR and the post-op CT. Blue=lead. Turquoise=Thalamus. Pink=STN. Orange=Caudate. Green=ventricles. **C.** Power spectrogram at a logarithmic scale of the non-normalized raw data recorded from 8 contacts of one DBS lead, re-referenced bipolar to the adjacent contact. The beta frequency range is highlighted with a grey background. A difference in baseline power between intra- and extra-STN contacts is evident, best shown between 140-160 Hz. **D.** The same spectrogram as in B, after normalization, to exclude inter-contact variation in baseline activity within the same STN. A prominent peak can be seen at the beta frequency (grey background), at the STN contacts, while the baseline power difference across contacts is no more evident. The contact with maximal beta power was located to the dorsal (motor) part of the STN. **E.** Color map of beta power recorded from all contacts of one example of the STN electrode according to their 3D AC-PC coordinates. Beta power was maximal at the dorsal border of the STN (dark red), lower in vSTN (yellow-orange) and much lower at contacts dorsal to the STN (blue). MCP=Midcommisural point. The color map is for normalized log power scale.

Journal Pre-proof

Table 2. Relative locations of contacts with maximal Beta power and STN trajectory length. A detailed description of the normalized (relative) locations of contacts with maximal (of all 7 bipolar contacts of the same lead) beta power, length of STN trajectory according to Microelectrode recordings (MER) and the number of lead contacts in the STN (according to MER and intra-op plan for implantation). Abbreviations: STN=Subthalamic nucleus.

Figure 2. Beta power at the STN vicinity is maximal at the dorsal Subthalamic nucleus. A. A scheme of the normalization method for the location of lead contacts (right), based on the MER (left). STN length was defined as 0-1, with zero is STN exit and 1 is STN entry. Five zones of normalized locations (0.5 each) were defined accordingly: zone 1=location 0-0.5, ventral half of STN; zone 2=location 0.5-1, dorsal half of STN; zone 3=location 1-1.5, just dorsal to the STN; zone 4=location 1.5-2, dorsal to zone 3; and zone 5=location >2, dorsal to zone 4. **B.** A plot of mean (highlighted color line) ± SEM (shaded color areas) of all recorded contacts' power spectrogram (at 0-60 Hz), separated by the contact's normalized location. The legend shows the color for each contact normalized location. **C.** A box plot of the median and range Beta power of all recorded contacts separated by their normalized location. A black asterisk shows a significant difference between groups. Red asterisks denote extreme data points, red lines denote median value, black error bars denote range (minimum and maximum values), blue boxes denote 25-75% of values. **D.** Histogram of the distribution of the normalized location of the contact with maximal Beta power.

Figure 3. Beta phase reversal is located at the dorsal Subthalamic nucleus. A. An example of a 500 ms bipolar LFP signal from one patient's hemisphere, band-pass filtered at the beta frequency, recorded simultaneously from contact pairs in all five location zones (two additional contacts in zone 4 and 5 were omitted for illustrative purposes). The reversal of the polarity of the signal can be seen between the ventral (blue) and dorsal (green) STN contacts. **B.** Circular analysis of the average beta phase shift, in degrees, of the filtered signal between contacts in the various locations from the same patient in A. Narrow distribution of complete reversal (180 degrees) can be depicted between ventral and dorsal STN (upper left trace). **C.** Distribution of the locations for beta phase reversal at all patients' STNs shows preference to the dSTN.

Figure 4. HFA power and beta-HFA phase-amplitude coupling co-localize with beta power to the dorsal Subthalamic nucleus. A. Left, Histogram showing the distribution of locations of contacts with maximal Beta bursts amplitude in each lead. **Right,** Histogram showing the distribution of locations of contacts with maximal Beta bursts duration in each lead. **B.** Correlation between maximal amplitude of Beta bursts in each lead and maximal HFA power (p=0.01). **C.** Phase amplitude coupling graphs for each normalized location. The color map represents the strength of PAC. Beta-HFA PAC is maximal at the dSTN contact (in yellow). **D.** Histogram showing the distribution of maximal PAC (for each patient's lead) across contact locations. In most leads, the maximal PAC was found at the dSTN. **E.** An example of a power spectrogram of the high frequency activity (HFA; 200-400 Hz) recorded simultaneously from all contacts of one patient's lead. The highest HFA peak (red) was detected at contact 3-4, localized at the dSTN. **F.** Histogram showing the distribution of maximal HFA power (for each patient's lead) across contact locations. In most leads, maximal power localized to the dorsal STN border. **G.** Correlation between the location of contact with maximal Beta power and location of contact with maximal PAC (p=0.02). H. Correlation between max PAC and contralateral on-off stim (both off med) UPDRS (p=0.01).

Figure 5

Beta power is co-localized with chronic stimulation and correlates with PD severity. A. Histogram of the preferred locations for chronic DBS stimulation in all patients. The most common location for chronic stimulation is dSTN. **B.** Correlation between maximal beta power (of all contacts in each lead) and pre-operative off medication UPDRS III points (only points related to contralateral limb bradykinesia and rigidity). A significant positive correlation is noted (p=0.02).

Journal Pre-proof

Acknowledgments and Funding

We are grateful to Robin and Harold Vinegar for their support of this work via the Vinegar family foundation, Houston, Texas, USA.

Journal Pre-proof

References

Alavi, M., J. O. Dostrovsky, M. Hodaie, A. M. Lozano, and W. D. Hutchison. 2013. 'Spatial extent of beta oscillatory activity in and between the subthalamic nucleus and substantia nigra pars reticulata of Parkinson's disease patients', *Exp Neurol*, 245: 60-71.

Buzsaki, G., and A. Draguhn. 2004. 'Neuronal oscillations in cortical networks', *Science*, 304: 1926-9.

Canolty, R. T., E. Edwards, S. S. Dalal, M. Soltani, S. S. Nagarajan, H. E. Kirsch, M. S. Berger, N. M. Barbaro, and R. T. Knight. 2006. 'High gamma power is phase-locked to theta oscillations in human neocortex', *Science*, 313: 1626-8.

Chen, C. C., Y. T. Hsu, H. L. Chan, S. M. Chiou, P. H. Tu, S. T. Lee, C. H. Tsai, C. S. Lu, and P. Brown. 2010. 'Complexity of subthalamic 13-35 Hz oscillatory activity directly correlates with clinical impairment in patients with Parkinson's disease', *Exp Neurol*, 224: 234-40.

Cole, S. R., R. van der Meij, E. J. Peterson, C. de Hemptinne, P. A. Starr, and B. Voytek. 2017. 'Nonsinusoidal Beta Oscillations Reflect Cortical Pathophysiology in Parkinson's Disease', *J Neurosci*, 37: 4830-40.

Deffains, M., and H. Bergman. 2019. 'Parkinsonism-related beta oscillations in the primate basal ganglia networks - Recent advances and clinical implications', *Parkinsonism Relat Disord*, 59: 2-8.

Deffains, M., L. Iskhakova, S. Katabi, S. N. Haber, Z. Israel, and H. Bergman. 2016. 'Subthalamic, not striatal, activity correlates with basal ganglia downstream activity in normal and parkinsonian monkeys', *Elife*, 5.

Eitan, R., R. R. Shamir, E. Linetsky, O. Rosenbluh, S. Moshel, T. Ben-Hur, H. Bergman, and Z. Israel. 2013. 'Asymmetric right/left encoding of emotions in the human subthalamic nucleus', *Front Syst Neurosci*, 7: 69.

Feng, H., P. Zhuang, M. Hallett, Y. Zhang, J. Li, and Y. Li. 2016. 'Characteristics of subthalamic oscillatory activity in parkinsonian akinetic-rigid type and mixed type', *Int J Neurosci*, 126: 819-28.

Foffani, G., A. Priori, M. Egidi, P. Rampini, F. Tamma, E. Caputo, K. A. Moxon, S. Cerutti, and S. Barbieri. 2003. '300-Hz subthalamic oscillations in Parkinson's disease', *Brain*, 126: 2153-63.

Galati, S., P. Stanzione, V. D'Angelo, E. Federe, F. Marzetti, G. Sancesario, T. Procopio, and A. Stefani. 2009. 'The pharmacological blockade of medial forebrain bundle induces an acute pathological synchronization of the cortico-subthalamic nucleus-globus pallidus pathway', *J Physiol*, 587: 4405-23.

Gerber, E. M., B. Sadeh, A. Ward, R. T. Knight, and L. Y. Deouell. 2016. 'Non-Sinusoidal Activity Can Produce Cross-Frequency Coupling in Cortical Signals in the Absence of Functional Interaction between Neural Sources', *PLoS One*, 11: e0167351.

Hohlefeld, F. U., F. Ehlen, H. O. Tiedt, L. K. Krugel, A. Horn, A. A. Kuhn, G. Curio, F. Klostermann, and V. V. Nikulin. 2015. 'Correlation between cortical and subcortical neural dynamics on multiple time scales in Parkinson's disease', *Neuroscience*, 298: 145-60.

Hohlefeld, F. U., C. Huchzermeyer, J. Huebl, G. H. Schneider, G. Nolte, C. Brucke, T. Schonecker, A. A. Kuhn, G. Curio, and V. V. Nikulin. 2013. 'Functional and effective connectivity in subthalamic local field potential recordings of patients with Parkinson's disease', *Neuroscience*, 250: 320-32.

Horn, A., W. J. Neumann, K. Degen, G. H. Schneider, and A. A. Kuhn. 2017. 'Toward an electrophysiological "sweet spot" for deep brain stimulation in the subthalamic nucleus', *Hum Brain Mapp*, 38: 3377-90.

Hyafil, A. 2017. 'Disharmony in neural oscillations', *J Neurophysiol*, 118: 1-3.

Kolb, R., A. Abosch, G. Felsen, and J. A. Thompson. 2017. 'Use of intraoperative local field potential spectral analysis to differentiate basal ganglia structures in Parkinson's disease patients', *Physiol Rep*, 5.

Kombos, T., O. Suess, B. C. Kern, T. Funk, T. Hoell, O. Kopetsch, and M. Brock. 1999. 'Comparison between monopolar and bipolar electrical stimulation of the motor cortex', *Acta Neurochir (Wien)*, 141: 1295-301.

Little, S., and P. Brown. 2012. 'What brain signals are suitable for feedback control of deep brain stimulation in Parkinson's disease?', *Ann N Y Acad Sci*, 1265: 9-24.

Lopez-Azcarate, J., M. Tainta, M. C. Rodriguez-Oroz, M. Valencia, R. Gonzalez, J. Guridi, J. Iriarte, J. A. Obeso, J. Artieda, and M. Alegre. 2010. 'Coupling between beta and high-frequency activity in the human subthalamic nucleus may be a pathophysiological mechanism in Parkinson's disease', *J Neurosci*, 30: 6667-77.

Lourens, M. A., H. G. Meijer, M. F. Contarino, P. van den Munckhof, P. R. Schuurman, S. A. van Gils, and L. J. Bour. 2013. 'Functional neuronal activity and connectivity within the subthalamic nucleus in Parkinson's disease', *Clin Neurophysiol*, 124: 967-81.

Marmor, O., D. Valsky, M. Joshua, A. S. Bick, D. Arkadir, I. Tamir, H. Bergman, Z. Israel, and R. Eitan. 2017. 'Local vs. volume conductance activity of field potentials in the human subthalamic nucleus', *J Neurophysiol*, 117: 2140-51.

Meidahl, A. C., C. K. E. Moll, B. C. M. van Wijk, A. Gulberti, G. Tinkhauser, M. Westphal, A. K. Engel, W. Hamel, P. Brown, and A. Sharott. 2019. 'Synchronised spiking activity underlies phase amplitude coupling in the subthalamic nucleus of Parkinson's disease patients', *Neurobiol Dis*, 127: 101-13.

Neumann, W. J., K. Degen, G. H. Schneider, C. Brucke, J. Huebl, P. Brown, and A. A. Kuhn. 2016. 'Subthalamic synchronized oscillatory activity correlates with motor impairment in patients with Parkinson's disease', *Mov Disord*, 31: 1748-51.

Ozkurt, T. E., M. Butz, M. Homburger, S. Elben, J. Vesper, L. Wojtecki, and A. Schnitzler. 2011. 'High frequency oscillations in the subthalamic nucleus: a neurophysiological marker of the motor state in Parkinson's disease', *Exp Neurol*, 229: 324-31.

Pina-Fuentes, D., M. Beudel, S. Little, P. Brown, D. L. M. Oterdoom, and J. M. C. van Dijk. 2019. 'Adaptive deep brain stimulation as advanced Parkinson's disease treatment (ADAPT study): protocol for a pseudo-randomised clinical study', *BMJ Open*, 9: e029652.

Plaha, P., Y. Ben-Shlomo, N. K. Patel, and S. S. Gill. 2006. 'Stimulation of the caudal zona incerta is superior to stimulation of the subthalamic nucleus in improving contralateral parkinsonism', *Brain*, 129: 1732-47.

Pogosyan, A., F. Yoshida, C. C. Chen, J. Martinez-Torres, T. Foltynie, P. Limousin, L. Zrinzo, M. I. Hariz, and P. Brown. 2010. 'Parkinsonian impairment correlates with spatially extensive subthalamic oscillatory synchronization', *Neuroscience*, 171: 245-57.

Pollok, B., D. Kamp, M. Butz, L. Wojtecki, L. Timmermann, M. Sudmeyer, V. Krause, and A. Schnitzler. 2013. 'Increased SMA-M1 coherence in Parkinson's disease - Pathophysiology or compensation?', *Exp Neurol*, 247: 178-81.

Rappel, P., O. Marmor, A. S. Bick, D. Arkadir, E. Linetsky, A. Castrioto, I. Tamir, S. A. Freedman, T. Mevorach, M. Gilad, H. Bergman, Z. Israel, and R. Eitan. 2018. 'Subthalamic theta activity: a novel human subcortical biomarker for obsessive compulsive disorder', *Transl Psychiatry*, 8: 118.

Rosa, M., G. Giannicola, D. Servello, S. Marceglia, C. Pacchetti, M. Porta, M. Sassi, E. Scelzo, S. Barbieri, and A. Priori. 2011. 'Subthalamic local field beta oscillations during ongoing deep brain stimulation in Parkinson's disease in hyperacute and chronic phases', *Neurosignals*, 19: 151-62.

Sanders, T. H., and D. Jaeger. 2016. 'Optogenetic stimulation of cortico-subthalamic projections is sufficient to ameliorate bradykinesia in 6-ohda lesioned mice', *Neurobiol Dis*, 95: 225-37.

Scheffer-Teixeira, R., and A. B. L. Tort. 2017. 'Unveiling Fast Field Oscillations through Comodulation', *eNeuro*, 4.

Schmidt, S. L., J. J. Peters, D. A. Turner, and W. M. Grill. 2020. 'Continuous deep brain stimulation of the subthalamic nucleus may not modulate beta bursts in patients with Parkinson's disease', *Brain Stimul*, 13: 433-43.

Shahlaie, K., P. S. Larson, and P. A. Starr. 2011. 'Intraoperative computed tomography for deep brain stimulation surgery: technique and accuracy assessment', *Neurosurgery*, 68: 114-24; discussion 24.

Sharott, A., P. J. Magill, D. Harnack, A. Kupsch, W. Meissner, and P. Brown. 2005. 'Dopamine depletion increases the power and coherence of beta-oscillations in the cerebral cortex and subthalamic nucleus of the awake rat', *Eur J Neurosci*, 21: 1413-22.

Shreve, L. A., A. Velisar, M. Malekmohammadi, M. M. Koop, M. Trager, E. J. Quinn, B. C. Hill, Z. Blumenfeld, C. Kilbane, A. Mantovani, J. M. Henderson, and H. Bronte-Stewart. 2017. 'Subthalamic oscillations and phase amplitude coupling are greater in the more affected hemisphere in Parkinson's disease', *Clin Neurophysiol*, 128: 128-37.

Starr, P. A. 2002. 'Placement of deep brain stimulators into the subthalamic nucleus or Globus pallidus internus: technical approach', *Stereotact Funct Neurosurg*, 79: 118-45.

Tamir, I., O. Marmor-Levin, R. Eitan, H. Bergman, and Z. Israel. 2017. 'Posterolateral Trajectories Favor a Longer Motor Domain in Subthalamic Nucleus Deep Brain Stimulation for Parkinson Disease', *World Neurosurg*, 106: 450-61.

Tinkhauser, G., A. Pogosyan, S. Little, M. Beudel, D. M. Herz, H. Tan, and P. Brown. 2017. 'The modulatory effect of adaptive deep brain stimulation on beta bursts in Parkinson's disease', *Brain*, 140: 1053-67.

Tinkhauser, G., A. Pogosyan, H. Tan, D. M. Herz, A. A. Kuhn, and P. Brown. 2017. 'Beta burst dynamics in Parkinson's disease OFF and ON dopaminergic medication', *Brain*, 140: 2968-81.

Toledo, J. B., J. Lopez-Azcarate, D. Garcia-Garcia, J. Guridi, M. Valencia, J. Artieda, J. Obeso, M. Alegre, and M. Rodriguez-Oroz. 2014. 'High beta activity in the subthalamic nucleus and freezing of gait in Parkinson's disease', *Neurobiol Dis*, 64: 60-5.

Tommasi, G., M. Fiorio, J. Yelnik, P. Krack, P. Sala, E. Schmitt, V. Fraix, L. Bertolasi, J. F. Le Bas, G. K. Ricciardi, A. Fiaschi, J. Theeuwes, P. Pollak, and L. Chelazzi. 2015. 'Disentangling the Role of Cortico-Basal Ganglia Loops in Top-Down and Bottom-Up Visual Attention: An Investigation of Attention Deficits in Parkinson Disease', *J Cogn Neurosci*, 27: 1215-37.

Tort, A. B., R. Komorowski, H. Eichenbaum, and N. Kopell. 2010. 'Measuring phase-amplitude coupling between neuronal oscillations of different frequencies', *J Neurophysiol*, 104: 1195-210.

van Wijk, B. C., M. Beudel, A. Jha, A. Oswal, T. Foltynie, M. I. Hariz, P. Limousin, L. Zrinzo, T. Z. Aziz, A. L. Green, P. Brown, and V. Litvak. 2016. 'Subthalamic nucleus phase-amplitude coupling correlates with motor impairment in Parkinson's disease', *Clin Neurophysiol*, 127: 2010-9.

van Wijk, B. C. M., A. Pogosyan, M. I. Hariz, H. Akram, T. Foltynie, P. Limousin, A. Horn, S. Ewert, P. Brown, and V. Litvak. 2017. 'Localization of beta and high-frequency oscillations within the subthalamic nucleus region', *Neuroimage Clin*, 16: 175-83.

Verhagen, R., D. G. Zwartjes, T. Heida, E. C. Wiegers, M. F. Contarino, R. M. de Bie, P. van den Munckhof, P. R. Schuurman, P. H. Veltink, and L. J. Bour. 2015. 'Advanced target identification in STN-DBS with beta power of combined local field potentials and spiking activity', *J Neurosci Methods*, 253: 116-25.

Wang, D. D., C. de Hemptinne, S. Miocinovic, J. L. Ostrem, N. B. Galifianakis, M. San Luciano, and P. A. Starr. 2018. 'Pallidal Deep-Brain Stimulation Disrupts Pallidal Beta Oscillations and Coherence with Primary Motor Cortex in Parkinson's Disease', *J Neurosci*, 38: 4556-68.

West, T., S. Farmer, L. Berthouze, A. Jha, M. Beudel, T. Foltynie, P. Limousin, L. Zrinzo, P. Brown, and V. Litvak. 2016. 'The Parkinsonian Subthalamic Network: Measures of Power, Linear, and Non-

linear Synchronization and their Relationship to L-DOPA Treatment and OFF State Motor Severity', *Front Hum Neurosci*, 10: 517.

Wichmann, T., H. Bergman, and M. R. DeLong. 2018. 'Basal ganglia, movement disorders and deep brain stimulation: advances made through non-human primate research', *J Neural Transm (Vienna)*, 125: 419-30.

Yang, A. I., N. Vanegas, C. Lungu, and K. A. Zaghloul. 2014. 'Beta-coupled high-frequency activity and beta-locked neuronal spiking in the subthalamic nucleus of Parkinson's disease', *J Neurosci*, 34: 12816-27.

Zaidel, A., A. Spivak, B. Grieb, H. Bergman, and Z. Israel. 2010. 'Subthalamic span of beta oscillations predicts deep brain stimulation efficacy for patients with Parkinson's disease', *Brain*, 133: 2007-21.

Zhong, W., M. Ciatipis, T. Wolfenstetter, J. Jessberger, C. Muller, S. Ponsel, Y. Yanovsky, J. Brankack, A. B. L. Tort, and A. Draguhn. 2017. 'Selective entrainment of gamma subbands by different slow network oscillations', *Proc Natl Acad Sci U S A*, 114: 4519-24.

Journal Pre-proof

	AGE	DISEASE DURATION (YRS)	GENDER	PRE-OP OFF MEDS UPDRS III (TOTAL)	PRE-OP OFF MEDS UPDRS III (HEMIBODY BR)	INTRA-OP RECORDED STN SIDE
PT 1	56	6	F	31	8	L
PT2	50	12	M	49	7	L
PT3	72	9	F	37	8	L
					12	R
PT4	66	11	F	59	17	L
					15	R
PT5	46	10	M	36	8	R
PT6	68	12	M	53	13	L
					13	R
PT7	70	10	M	39	11	L
					9	R
PT8	56	10	M	54	12	L

Table 1 **(2 column fitting table)**

Journal Pre-proof

Relative location of max Beta power contact	STN trajectory length (mm)	Number of contacts in STN
0.94	7.1	3
0.65	5.75	3
1.24	5.95	3
0.55	5	2
0.55	5	2
0.5	6.5	4
1.23	6.3	3
0.87	5.7	2
0.95	5.3	3
1.16	5.4	3
0.86	5.2	2
0.76	5.6	3

Table 2 **(1.5 column fitting table)**

Journal Pre-proof

Credit Author statement - individual contributions to the paper:

Idit Tamir – Conceptualization, Data curation, methodology, formal analysis, writing

Doris Wang – Formal analysis, review, and editing,

Witney Chen – methodology, data collection, review, and editing

Jill Ostrem – Data collection, review & editing

Philip Starr - Conceptualization, data collection, review & editing

Coralie de Hemptinne – conceptualization, data collection, supervision, methodology, review, and editing

Journal Pre-proof

Highlights

- Wide span 8 contact DBS leads localize beta oscillatory activity to the dorsal STN
- Dorsal STN is the main generator of beta oscillations at the STN vicinity
- Beta power, phase reversal and bursts are co-localized to the dorsal STN
- HFA and beta-HFA coupling (PAC) are maximal at and co-localized to the dSTN
- Beta power at stimulation contact is correlated with Parkinson's Disease severity

Journal Pre-proof